Structural and Dynamic Properties of a β-Hairpin-Forming Linear Peptide. 2. ^{13}C NMR Relaxation Analysis

Mark S. Friedrichs,[†] Terry R. Stouch,[‡] Robert E. Bruccoleri,[‡] Luciano Mueller,[†] and Keith L. Constantine*,[†]

Contribution from the Departments of Macromolecular NMR and Macromolecular Modeling, Bristol-Myers Squibb Pharmaceutical Research Institute, P.O. Box 4000, Princeton, New Jersey 08543-4000

Received June 22, 1995[⊗]

Abstract: In the preceding paper in this issue (K. L. Constantine et al. *J. Am. Chem. Soc.* **1995**, *117*, 10841−10854), the structural and dynamic properties of the β-hairpin forming linear peptide Y-Q-N-P-D-G-S-Q-A (one letter amino acid code; F. J. Blanco et al. *J. Am. Chem. Soc.* **1993**, *115*, 5887−5888) were characterized by molecular modeling using ensemble-averaged constraints. In this report, the dynamic behavior of the peptide backbone is further investigated by 2D $^{1}H-^{13}C$ NMR methods at natural ^{13}C abundance. The dynamics of the backbone methine $H^{\alpha}-C^{\alpha}$ sites were characterized by measurements of $\{^{1}H\}-^{13}C$ steady state NOEs, ^{13}C spin-lattice relaxation rates $R_1(C)$, ^{13}C spin−spin relaxation rates $R_2(C)$, relaxation rates of longitudinal two-spin order $R_{1zz}(H,C)$, and the spin−lattice relaxation rates of ^{13}C-attached protons $R_1(H)$. Relaxation observables were fit using model-free spectral density functions. The results of this analysis indicate relatively low mobility on a picosecond−nanosecond time scale for residues 2, 3, 4, and 5, intermediate flexibility for residue 7, and relatively high mobility on this time scale for residues 1, 8, and (especially) 9. Residue 9 may also experience motions on a nanosecond−millisecond time scale. An unrestrained, water-solvated molecular dynamics simulation of the peptide was also performed. This simulation included a 0.70 ns equilibration period followed by 1.40 ns of production dynamics at 278 K. Order parameters derived from the ^{13}C relaxation data are compared to order parameters extracted from the molecular dynamics simulation and to order parameters derived from the ensemble-averaged modeling results. The combined data suggest that the peptide may mimic a protein folding intermediate, with significantly populated hydrogen bonds and "loose" interactions among hydrophobic and terminal charged groups.

Introduction

The stable macrostates of polypeptides are a consequence of a complex balance between enthalpic and entropic effects.[1] In globular proteins, a cooperative interplay between hydrogen bonding, electrostatic and van der Waals interactions, the burial of nonpolar groups, and the accompanying entropy increase due to the release of bound solvent and counterions stabilizes the folded state. These are opposed by main-chain and side-chain configurational entropies and by noncovalent interactions between protein groups and the solvent.

Recently, a stable macrostate that is intermediate betwen the folded and denatured states has been observed for a number of proteins under appropriate conditions.[2] Termed the "molten globule", this state is generally characterized by increased mobility of hydrophobic residues relative to the folded state and by solvent exposure of hydrophobic residues that is intermediate between that of the folded and denatured states. Also, molten globules generally contain a significant amount of hydrogen-bonded secondary structure. Thus, in the molten globule state, the hydrophobic side chains gain conformational entropy without a complete loss of van der Waals interactions with other apolar groups, and many hydrogen bonding interactions are maintained.

While the direct study of the structural, dynamic, and thermodynamic properties of actual protein folding intermediates is indispensible for the characterization of these systems, investigations of simpler model systems are also important. Simpler systems can often be studied more readily and at a higher level of detail. We have undertaken a detailed study of the linear peptide Y-Q-N-P-D-G-S-Q-A, which adopts a highly populated β-hairpin conformation in aqueous solution at 5 °C.[3] The structural and dynamic properties have been investigated using restrained, ensemble-averaged simulated annealing calculations (preceding article in this issue). In this article, the dynamic behavior of the peptide is investigated by natural abundance ^{13}C NMR relaxation measurements and by an unrestrained, water-solvated molecular dynamics (MD) simulation. Order parameters derived from the ensemble-averaged structures, the relaxation data, and the MD simulation are compared. The applicability of the model-free approach and issues concerning the order parameter comparisons are discussed.

[†] Department of Macromolecular NMR.

[‡] Department of Macromolecular Modeling.

[⊗] Abstract published in *Advance ACS Abstracts,* November 1, 1995.

(1) (a) Privalov, P. L.; Gill, S. J. *Adv. Prot. Chem.* **1988**, *39*, 191−234. (b) Dill, K. A. *Biochemistry* **1990**, *29*, 7133−7155. (c) Pace, C. N. *Trends Biochem. Sci.* **1990**, *15*, 14−17. (d) Freire, E.; Murphy, K. P. *J. Mol. Biol.* **1991**, *222*, 687−698. (e) Murphy, K. P.; Freire, E. *Adv. Prot. Chem.* **1992**, *43*, 313−361. (f) Sneddon, S. F.; Tobias, D. J. *Biochemistry* **1992**, *31*, 2842−2846.

(2) (a) Kuwajima, K. *J. Mol. Biol.* **1977**, *114*, 241−258. (b) Dolgikh, D. A.; Gilmanshin, R. I.; Brazhnikov, V. E.; Bychkova, G. V.; Semisotnov, G. V.; Venyaminov, S.; Ptitsyn, O. B. *FEBS Lett.* **1981**, *136*, 311−315. (c) Ohgushi, M.; Wada, A. *FEBS Lett.* **1983**, *164*, 21−24. (d) Brems, D. N.; Havel, H. A. *Proteins: Struct. Funct. Genet.* **1989**, *5*, 93−95. (e) Goto, Y.; Fink, A. L. *Biochemistry* **1989**, *28*, 945−952. (f) Kuwajima, K. *Proteins: Struct. Funct. Genet.* **1989**, *6*, 87−103. (g) Dryden, D.; Weir, M. P. *Biochim. Biophys. Acta* **1991**, *1078*, 94−100. (h) Hua, Q.-X.; Kochoyan, M.; Weiss, M. A. *Proc. Natl. Acad. Sci. U.S.A.* **1992**, *89*, 2379−2383. (i) Kuroda, Y.; Kidokoro, S.; Wada, A. *J. Mol. Biol.* **1992**, *223*, 1139−1153. (j) Haynie, D. T.; Freire, E. *Proteins: Struct. Funct. Genet.* **1993**, *16*, 115−140. (k) Peng, X.; Jonas, J.; Silva, J. L. *Biochemistry* **1994**, *33*, 8323−8329.

(3) Blanco, F. J.; Jimenez, M. A.; Herranz, J.; Rico, M.; Santoro, J.; Nieto, J. L. *J. Am. Chem. Soc.* **1993**, *115*, 5887−5888.

0002-7863/95/1517-10855$09.00/0

Background

For an NMR-based structure determination, the failure of any single structure to satisfy the experimental NOE distance and J-coupling data provides indirect evidence for conformational dynamics (preceding article in this issue, and references therein). Direct evidence for polypeptide dynamics can be obtained from ^{13}C relaxation measurements.[4] Using inverse detected two-dimensional (2D) $^{1}H-^{13}C$ NMR methods (see **Materials and Methods**), five relaxation observables were measured for the methine $^{1}H-^{13}C$ groups of Y-Q-N-P-D-G-S-Q-A: the ^{13}C spin–lattice relaxation rates $R_1(C)$, the ^{13}C spin–spin relaxation rates $R_2(C)$, the $\{^{1}H\}-^{13}C$ steady state NOEs, the relaxation rates of longitudinal two-spin order $R_{1zz}(H,C)$, and the spin–lattice relaxation rates of ^{13}C-attached protons $R_1(H)$. For methine $^{1}H-^{13}C$ spin systems, the dipolar and chemical shielding anisotropy (CSA) contributions to the relaxation observables are given by[5,6]

$$R_1(C) = 1/T_1(C) = d^2[J(\omega_H-\omega_C) + 3J(\omega_C) + 6J(\omega_H+\omega_C)] + c^2J(\omega_C) \quad (1)$$

$$R_2(C) = 1/T_2(C) = 0.5d^2[4J(0) + J(\omega_H-\omega_C) + 3J(\omega_C) + 6J(\omega_H) + 6J(\omega_H+\omega_C)] + c^2[4J(0) + 3J(\omega_C)]/6 \quad (2)$$

$$NOE = 1 + T_1(C)(\gamma_H/\gamma_C)d^2[6J(\omega_H+\omega_C) - J(\omega_H-\omega_C)] \quad (3)$$

$$R_{1zz}(H,C) = 1/T_{1zz}(H,C) = d^2[3J(\omega_C) + 3J(\omega_H)] + c^2J(\omega_C) + \rho_{HH} \quad (4)$$

$$R_1(H) = 1/T_1(H) = d^2[J(\omega_H-\omega_C) + 3J(\omega_H) + 6J(\omega_H+\omega_C)] + \rho_{HH} \quad (5)$$

In these expressions, ω_H and ω_C are the Larmor frequencies for ^{1}H and ^{13}C (3.769×10^9 and 9.479×10^8 rad/s, respectively, in this study), γ_H and γ_C are the ^{1}H and ^{13}C magnetogyric ratios, and c^2 and d^2 are the products of physical constants relevant to the CSA and dipolar relaxation mechanisms, respectively. The dipolar constant d^2 is given by $(1/40)\gamma_H^2\gamma_C^2h^2\pi^{-2}\langle r_{CH}^{-3}\rangle^2$, where h is Planck's constant and r_{CH} is the length of the CH bond (1.09 Å). The CSA constant c^2 is given by $(2/15)\omega_C^2(\sigma_{||} - \sigma_\perp)^2$, where $\sigma_{||}$ and $\sigma_\perp$ are the parallel and perpendicular components of the $^{13}C^\alpha$ chemical shift tensor ($\sigma_{||} - \sigma_\perp \sim 25$ ppm[7]). ρ_{HH} is the contribution to the spin–lattice relaxation rate of the ^{13}C-attached proton due to dipole–dipole interactions with other surrounding protons. The spectral density functions, $J(\omega)$, are the Fourier transforms of the autocorrelation functions of the CH vectors. Exchange contributions to $R_2(C)$, due to motions on the microsecond–millisecond time scale, are treated by adding a third term R_{2ex} ($= 1/T_{2x}$) to eq 2.

Three relaxation observables – $R_1(C)$, $R_2(C)$, and the $\{^{1}H\}-^{13}C$ NOE–do not depend on ρ_{HH}. Since ρ_{HH} reflects $^{1}H-^{1}H$ dipolar interactions, it cannot be cast in terms of spectral density functions involving the CH vectors. A fourth relaxation observable that is independent of ρ_{HH} is obtained by taking the difference

$$\Delta_z \equiv R_{1zz}(H,C) - R_1(H) = d^2[3J(\omega_C) - J(\omega_H-\omega_C) - 6J(\omega_H+\omega_C)] + c^2J(\omega_C) \quad (6)$$

For macromolecules, the $3J(\omega_C)$ term dominates, and thus the difference will be positive.

Motional parameters can be derived using model-free spectral density functions.[8] In this study, three functional forms were used to fit the relaxation data. In order of increasing complexity, these are as follows

$$J(\omega) = \mathbf{S}^2\tau_r/(1 + \omega^2\tau_r^2) \quad (7)$$

$$J(\omega) = \mathbf{S}^2\tau_r/(1 + \omega^2\tau_r^2) + (1 - \mathbf{S}^2)\tau/(1 + \omega^2\tau^2) \quad (8)$$

$$J(\omega) = S_f^2\mathbf{S}_s^2\tau_r/(1 + \omega^2\tau_r^2) + S_f^2(1 - \mathbf{S}_s^2)\tau_s'/(1 + \omega^2\tau_s'^2) \quad (9)$$

In these expressions, $\mathbf{S}^2$ is the total generalized order parameter (which depends on the amplitudes of picosecond–nanosecond motions), τ_r is the overall molecular rotational correlation time, τ is an effective correlation time resulting from internal motions characterized by a single internal correlation time τ_e($1/\tau = 1/\tau_e + 1/\tau_r$), S_f^2 and $\mathbf{S}_s^2$ are order parameters corresponding to fast and slow internal picosecond–nanosecond motions with time scales differing by at least an order of magnitude, respectively (note: $\mathbf{S}^2 = S_f^2\mathbf{S}_s^2$), and τ_s' is an effective correlation time given by $1/\tau_s' = 1/\tau_s + 1/\tau_r$, where τ_s is the correlation time associated with slower internal motions. Equation 9 is based on the assumption that the correlation time for the faster internal motions is less than ~20 ps.[8d] The τ_r value is treated either as a global parameter determined by a preliminary global fitting of the data or as a local parameter for each individual residue. When τ_r is treated as a global parameter, eqs 7, 8, and 9 contain one, two, and three adjustable parameters, respectively. In some cases, a fourth parameter (R_{2ex}) is required. With four independent observables, a four-parameter fit is feasible.

Materials and Methods

NMR Spectroscopy. All spectra were recorded on a Varian Unity 600 NMR spectrometer operating at 599.91 MHz proton frequency, using a ~15 mM sample (0.60 mL) of the peptide prepared in 99.999% $^{2}H_2O$ (Isotec, Inc, Miamisburg, OH). The temperature was set to 5 °C for all experiments. ^{1}H chemical shifts were referenced to the residual $^{1}H^{2}HO$ resonance, which is at 5.00 ppm relative to an external TSP ((trimethylsilyl)[2,2,3,3-$^{2}H_4$]propionate) standard. The ^{13}C chemical shifts were referenced indirectly to TSP.[9]

Spectra were acquired with the ^{1}H and ^{13}C carrier frequencies set to 5.00 and 50.6 ppm, respectively, and with spectral widths of 7000 Hz (^{1}H) and 2000 Hz (^{13}C). For each spectrum, 36 t_1 increments were acquired, and 32 scans were collected per t_1 increment for all spectra except the $\{^{1}H\}-^{13}C$ NOE(on) and $\{^{1}H\}-^{13}C$ NOE(off) experiments, which were acquired with 64 scans per t_1 increment. Complex data points (2048) were collected along t_2. Removal of the residual $^{1}H^{2}HO$

(4) (a) Doddrell, D.; Glushko, V.; Allerhand, A. *J. Chem. Phys.* **1972**, *56*, 3683–3689. (b) Kitamaru, R. *NMR in Stereochemical Analysis* VCH Publishers, Inc.: New York, 1986; pp 75–124. (c) Nirmala, N. R.; Wagner, G. *J. Am. Chem. Soc.* **1988**, *110*, 7557–7558. (d) Dellwo, M. J.; Wand, A. *J. Am. Chem. Soc.* **1989**, *111*, 4571–4578. (e) Nirmala, N. R.; Wagner, G. *J. Magn. Reson.* **1989**, *82*, 659–661. (f) Palmer, A. G. III; Rance, M.; Wright, P. E. *J. Am. Chem. Soc.* **1991**, *113*, 4371–4380. (g) Kelsh, L. P.; Ellena, J. F.; Cafisco, D. S. *Biochemistry* **1992**, *31*, 5136–5144.

(5) Abragam, A. *The Principles of Nuclear Magnetism* Clarendon Press: Oxford, England, 1961.

(6) (a) Peng, J. W.; Wagner, G. *J. Magn. Reson.* **1992**, *98*, 308–332. (b) Peng, J. W.; Wagner, G. *Biochemistry* **1992**, *31*, 8571–8586.

(7) (a) Naito, A.; Ganapathy, S.; Akasaka, K.; McDowell, C. A. *J. Chem. Phys.* **1981**, *74*, 3190–3197. (b) Janes, N.; Ganapathy, S.; Oldfield, E. *J. Magn. Reson.* **1983**, *54*, 111–121. (c) Naito, A.; Ganapathy, S.; Raghunathan, P.; McDowell, C. A. *J. Chem. Phys.* **1983**, *79*, 4173–4182. (d) Naito, A.; McDowell, C. A. *J. Chem. Phys.* **1983**, *81*, 4795–4803.

(8) (a) Lipari, G.; Szabo, A. *J. Am. Chem. Soc.* **1982**, *104*, 4546–4559. (b) Lipari, G.; Szabo, A. *J. Am. Chem. Soc.* **1982**, *104*, 4559–4570. (c) Clore, G. M.; Szabo, A.; Bax, A.; Kay, L. E.; Driscoll, P. C.; Gronenborn, A. M. *J. Am. Chem. Soc.* **1990**, *112*, 4989–4991. (d) Clore, G. M.; Driscoll, P. C.; Wingfield, P. T.; Gronenborn, A. M. *Biochemistry* **1990**, *29*, 7387–7401.

(9) Fairbrother, W. J.; Palmer, A. G.; Rance, M.; Reizer, J.; Saier, M. H., Jr.; Wright, P. E. *Biochemistry* **1992**, *31*, 4413–4425.

resonance was achieved by on-resonance low-power irradiation during the recycle delays. All data sets were collected in an interleaved fashion (i.e., with the relaxation time delays incremented within the t_1 increments) in order to minimize possible errors associated with sample or spectrometer instabilities.

The ^{13}C $T_1(C)$ and $T_2(C)$ relaxation times and $\{^1H\}-^{13}C$ NOE values were determined using published pulse sequences.[10] A recycle delay of 2.4 s was used for the $T_1(C)$ and $T_2(C)$ data sets, while a 4.0 s recycle delay was used for the $\{^1H\}-^{13}C$ NOE data. For the T_1 data, ten inversion-recovery delays (5.0, 60.1, 110.2, 150.3, 200.4, 250.5, 300.6, 350.7, 400.8, and 501.0 ms) were used. CPMG delays of 6.4, 57.6, 108.8, 160.0, 211.2, 262.4, 313.6, 364.8, 416.0, and 467.2 ms were employed. ^{13}C $T_{1zz}(H,C)$ relaxation times were evaluated using a gradient-enhanced version of the published pulse sequence.[10b] This pulse sequence contains a 180° ^1H pulse in the center of the relaxation delay; this reduces the effects of cross-correlation between dipolar and CSA relaxation mechanisms.[11] Inversion-recovery delays of 20, 40, 60, 80, 100, 150, 200, 250, 350, and 500 ms were used for the T_{1zz} experiments. A gradient-enhanced version of a published pulse sequence[6a] for measuring $T_1(H)$ was also used, with relaxation delays of 30, 60, 90, 120, 180, 240, 300, 400, 500, and 700 ms. The gradient-enhanced pulse sequences used to determine the $T_{1zz}(H,C)$ and $T_1(H)$ relaxation times are given in the supplementary material.

The NMR spectra were processed with cosine-bell squared and cosine-bell apodization functions applied to the t_1 and t_2 time-domain data, respectively. The time-domain data were zero-filled and Fourier transformed to yield 128 real (F_1) by 2048 real (F_2) frequency-domain data point matrices. The baseline was flattened using a recently developed routine.[12]

Analysis of Relaxation Data. The $\{^1H\}-^{13}C$ steady state NOE values were determined by evaluating the ratio of crosspeak heights from experiments recorded with and without ^1H saturation (NOE = I_{sat}/I_{unsat}). Errors estimates for the NOE values were derived from the RMS baseline noise in the spectra. ^{13}C $T_1(C)$, $T_2(C)$, and $T_{1zz}(H,C)$ values were determined from a nonlinear least-squares fitting of the data to exponential decays

$$I(t) = I(0)\exp(-t/T_x), \quad x = 1, 2, 1zz \tag{10}$$

by minimization of χ^2, which is given by

$$\chi^2 = \sum[I(T_{xi}^e) - I(T_{xi}^c)]^2/\sigma_i^2, \quad x = 1, 2, 1zz \tag{11}$$

where superscripts "e" and "c" denote the experimental and calculated peak intensity of data point i, respectively, and σ_i is the experimental uncertainty in the intensity. The errors in the relaxation times were estimated by generating simulated data sets from a Gaussian distribution of the crosspeak intensities; the mean of the distribution was set to the measured heights, and the standard deviation was set to the root-mean-square baseline noise plus 1% of the peak height at the shortest relaxation delay.[13] The 1% is added in order to avoid underestimating the errors of the more intense peaks. A total of 500 simulated data sets for each relaxation time fitting were produced; the standard deviations of the mean relaxation times were then determined. The $R_1(H)$ data (eq 5) were treated differently since, in principle, nonexponential decays are expected.[6] (Nonexponential decays may also occur for $R_{1zz}(H,C)$, but ρ_{HH} makes a relatively small contribution to $R_{1zz}(H,C)$, and in practice these data fit exponential decays very well—see **Results**.) Approximate values of $R_1(H)$ can be obtained by fitting these data to exponential decays or by fitting the shorter mixing time data to a Taylor series expansion of the relaxation matrix.[6] We used both procedures, and took $R_1(H)$ to be the mean value from the two procedures. The standard deviation was set equal to either the error σ_i, or to half the difference in the values obtained from the exponential and Taylor series fits, whichever was larger.

After determining the global τ_r (see **Results**), model-free parameters and error estimates were independently derived for each residue by numerical fits to their respective relaxation data.[14] The $T_1(C)$, $T_2(C)$, and NOE observables were included in all fits, while fits were performed both with and without Δ_z (eq 6). The fits were performed using the Levenberg–Marquardt algorithm[14] to minimize χ^2

$$\chi^2 = \sum[(X^e - X^c)/\sigma_x]^2 \tag{12}$$

where the superscripts "e" and "c" refer to the experimental and calculated relaxation observables, respectively, and σ_x is the uncertainty in the relaxation observable X. The sum is over all relaxation observables for a given residue. The errors in the fitted model-free parameters were subsequently estimated by generating 100 simulated data sets of relaxation observables from Gaussian distributions. The mean of the distributions was set to the calculated relaxation observable, and the standard deviation was set to their estimated error.

To select the model-free parameters to include in the fit, we have adopted the following protocol, which largely eliminates the need for subjective decisions[8d,13,15] regarding model free parameters to include. Initially, for all residues, the relaxation observables are fit using eq 7 without a R_{2ex} term. This constitutes a one-parameter ($\mathbf{S}^2$) fit. If, for a given residue, this simple model reproduces all of the relaxation observables within their errors (within the 95% confidence interval defined by an F-test), the analysis is concluded. If the observables are not reproduced, then *two* two-parameter fits are performed: one with eq 8 ($\mathbf{S}^2$ and τ_e), and one with eq 7 ($\mathbf{S}^2$) and R_{2ex}. If either or both of these models reproduce all of the relaxation observables within their errors, the analysis is concluded. If the observables are not reproduced, then *two* three-parameter fits are performed: one with eq 9 (S_f^2, $\mathbf{S}_s^2$ and τ_s) and one with eq 8 ($\mathbf{S}^2$ and τ_e) and R_{2ex}. Up to this point, the procedure can be applied using three ($T_1(C)$, $T_2(C)$, and NOE) or four ($T_1(C)$, $T_2(C)$, NOE, and Δ_2) relaxation observables. If an adequate fit is not obtained with either of the three-parameter models, and if all four relaxation observables have been measured, then a four-parameter fit (eq 9 and R_{2ex}) is performed. An analysis is also performed treating τ_r as a local (adjustable) parameter. This precludes use of eq 9 and R_{ex} in the cases of three and four observables. In the case of three observables, the most complex fits possible are eq 7 with R_{2ex} or eq 8 without R_{2ex}. In all cases, the model free parameters are examined to determine if they fall within physically reasonable ranges: $1 \geq \mathbf{S}^2 \geq 0$, $\tau_e < \tau_r$, $\tau_s < \tau_r$, and $R_{2ex} \geq 0$.

Molecular Dynamics Simulation. Energy minimization and MD calculations were performed with version 2.6 of the DISCOVER program (Biosym Technologies, San Diego, CA) running on a Cray YMP-2 supercomputer.

The starting conformation of the Y-Q-N-P-D-G-S-Q-A peptide used was a representative member taken from the set of structures generated with X-PLOR (accompanying article). The peptide (126 atoms) was placed in a 24 Å × 24 Å × 24 Å box containing 389 flexible SPC H_2O molecules,[16] yielding a system with 1293 atoms in total. Prior to running the MD simulation, the entire system was subjected to 2000 steps of steepest descents energy minimization.

The MD simulation was executed in the NVT ensemble using cubic periodic boundary conditions.[17] Snapshots from the trajectory were saved every 0.2 ps. The peptide was slowly heated from 50 to 278 K over 0.70 ns of equilibration; this was followed by 1.40 ns of production dynamics at 278 K. Integration of the classical equations of motion was accomplished using the Verlet algorithm,[18] with a timestep of 1.0 fs. A 15.0 Å cutoff distance was used for the nonbonded interactions,

(10) (a) Kay, L. E.; Torchia, D. A.; Bax, A. *Biochemistry* **1989**, *28*, 8972–8979. (b) Kay, L. E.; Nicholson, L. K.; Delaglio, F.; Bax, A.; Torchia, D. A. *J. Magn. Reson.* **1992**, *97*, 359–375.

(11) (a) Boyd, J.; Hommel, U.; Campbell, I. D. *Chem. Phys. Lett.* **1990**, *175*, 477–482. (b) Wagner, G.; Hyberts, S.; Peng, J. W. *NMR of Proteins*; CRC Press, Boca Raton, FL, 1993; pp 220–257.

(12) Friedrichs, M. S. *J. Biomolec. NMR* **1995**, *5*, 147–153.

(13) Constantine, K. L.; Friedrichs, M. S.; Bell, A. J.; Lavoi, T. B.; Mueller, L.; Metzler, W. J. *FEBS Lett.* **1993**, *336*, 457–461.

(14) Press, W. H.; Flannery, B. P.; Teukolsky, S. A.; Vetterling, W. T. *Numerical Recipies: The Art of Scientific Computing*; Cambridge University Press: U.K., 1989.

(15) Constantine, K. L.; Friedrichs, M. S.; Goldfarb, V.; Jeffrey, P. D.; Sheriff, S.; Mueller, L. *Proteins: Struct. Funct. Genetics* **1993**, *15*, 290–311.

(16) Avbelj, F.; Moult, J.; Kitson, D. H.; James, M. N.; Hagler, A. T. *Biochemistry* **1990**, *29*, 8658–8676.

(17) Allen, M. P.; Tildesley, D. J. *Computer Simulations of Liquids*; Oxford University Press: New York, 1987; pp 23–32.

(18) Verlet, L. *Phys. Rev.* **1967**, *159*, 98–103.

Table 1. Relaxation Observables for the Methine $H^{\alpha}-C^{\alpha}$ Groups of Y-Q-N-P-D-G-S-Q-A at 5 °C, pH 5.5

residue	NOE	$R_1(C)^a$	R_2 (C)	R_{1zz}(H,C)	R_1(H)	Δ_z
Tyr-1	1.62 ± 0.03	3.21 ± 0.07	4.71 ± 0.11	3.47 ± 0.08	2.09 ± 0.07	1.38 ± 0.11
Gln-2	1.39 ± 0.04	3.53 ± 0.09	5.34 ± 0.14	3.79 ± 0.10	2.08 ± 0.09	1.71 ± 0.14
Asn-3	1.39 ± 0.10	3.80 ± 0.20	6.30 ± 0.48			
Pro-4	1.37 ± 0.04	3.37 ± 0.08	5.56 ± 0.15	3.66 ± 0.09	1.82 ± 0.06	1.84 ± 0.11
Asp-5	1.35 ± 0.03	3.57 ± 0.08	5.61 ± 0.13	3.86 ± 0.09	1.66 ± 0.06	2.20 ± 0.11
Ser-7	1.43 ± 0.02	3.34 ± 0.07	5.11 ± 0.10	3.75 ± 0.08	1.92 ± 0.07	1.83 ± 0.11
Gln-8	1.48 ± 0.04	3.39 ± 0.09	4.63 ± 0.13	3.60 ± 0.09	1.95 ± 0.06	1.65 ± 0.11
Ala-9	1.79 ± 0.04	2.35 ± 0.07	5.31 ± 0.14	2.34 ± 0.07	1.52 ± 0.06	0.82 ± 0.09

[a] All relaxation rates are given in s^{-1}.

which were updated every 50 iterations. No shifting or switching functions were used, since a relatively large cutoff distance was employed. The simulation temperature was maintained by velocity rescaling.

Calculation of Structure-Based Generalized Order Parameters. In order to compare the extent of conformational sampling indicated by the ^{13}C relaxation data with that observed in the MD simulation (see above) and in sets of structures generated by NMR-based modeling (preceding article in this issue), generalized order parameters for the $C^{\alpha}-H^{\alpha}$ vectors were computed according to[8a]

$$S^2 = \langle P_2[\mu_i\mu_j]\rangle = [(n/2)(n-1)]^{-1}\sum_{i\neq j} P_2[\mu_i\mu_j] \qquad (13)$$

where $P_2(x)$ is the second Legendre polynomial ($P_2(x) = (3x^2 - 1)/2$), μ_i and μ_j are unit vectors parallel to the vector of interest in structures i and j, respectively, and n is the number of structures. For analysis of an MD trajectory, n is the number of snapshots in a specified time window. For a given set of structures, the individual conformers were all superimposed on to a molecular reference frame (the corresponding mean backbone-atom coordinates) before applying eq 13.

Results

Determination of the Primary Relaxation Observables. The $^1H^{\alpha}-^{13}C^{\alpha}$ crosspeaks of all eight residues with methine $H^{\alpha}-C^{\alpha}$ groups are well-resolved in the 2D $^1H-^{13}C$ correlation spectra. An example is given in Figure 1, which shows the $^1H^{\alpha}-^{13}C^{\alpha}$ region of one of the 2D spectra used for determining the $R_2(C)$ relaxation rates. Note that the $^{13}C^{\alpha}$ resonances of Asp-5 and Ala-9 overlap severely, precluding the use of simpler 1D methods for measuring the ^{13}C relaxation rates. The relaxation observables derived from the 2D spectra, discussed in the following paragraphs, are reported Table 1.

Fits of the $R_1(C)$ values were obtained for all eight residues using all 10 time points. These data yielded good fits to exponential decays. With the exception of Asn-3, all residues have maximum errors between the experimental and best-fit intensities that are ≤3% of the corresponding equilibrium magnetization. Asn-3 displays relatively weak crosspeaks due to the proximity of its resonance to the residual $^1H^2HO$ resonance. This residue yields a slightly poorer (but still adequate) $R_1(C)$ fit, with a maximum error between the experimental and best-fit peak intensities of 5%.

$R_2(C)$, $R_1(H)$, and $R_{1zz}(H,C)$ values were fit to exponential decays using all 10 time points for all residues except Asn-3. The $R_2(C)$ fit for Asn-3 was performed using the first six time points, and adequate fits of the $R_1(H)$ and $R_{1zz}(H,C)$ data for Asn-3 could not be obtained due to the severe attenuation of its $^1H^{\alpha}-^{13}C^{\alpha}$ crosspeak in these spectra. All residues have maximum errors between the experimental and best-fit peak intensities that are ≤4% for the $R_2(C)$ data, and all residues excluding Asn-3 have maximum errors between the experimental and best-fit peak intensities that are ≤2% for the $R_{1zz}(H,C)$ and $R_1(H)$ data. Examples of the exponential fits to the $R_{1zz}(H,C)$ and $R_1(H)$ data are given in Figures 2 and 3A, respectively. Using only the first seven time points, the $R_1(H)$ data were also fit to a second-order Taylor series expansion of the relaxation matrix. Examples of $R_1(H)$ data fit to the Taylor expansion are given in Figure 3B. This functional form also fit the data very well, with all fitted residues showing maximum errors ≤2%. The difference in the $R_1(H)$ relaxation rates between the fits using the two functional forms was ≤10%. Table 1 reports the average values. From the table, the largest $\{^1H\}-^{13}C$ NOEs and the smallest $R_1(C)$ and Δ_z relaxation rates are observed for the terminal residues Tyr-1 and Ala-9. Qualitatively, these results indicate these residues, especially Ala-9, are highly mobile on a picosecond–nanosecond time scale.

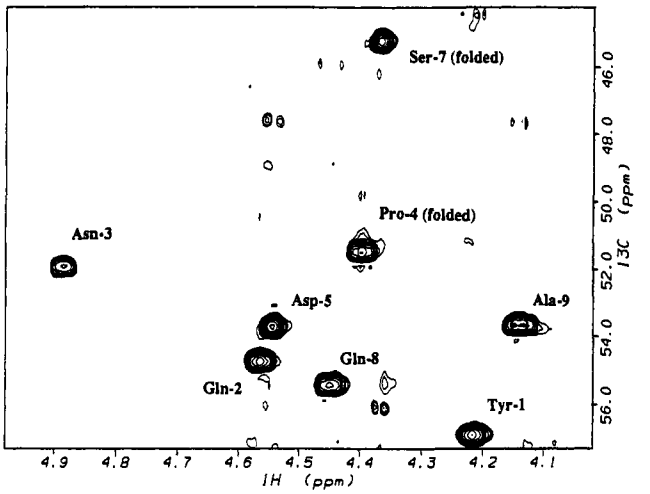

Figure 1. Example region of a 2D $^1H-^{13}C$ correlation spectrum used for deriving C^{α} $R_2(C)$ relaxation rates. The $H^{\alpha}-C^{\alpha}$ crosspeaks for all residues except Gly-6 are labeled. The CPMG delay used for this spectrum was 6.4 ms. The peptide concentration was approximately 15 mM in 100% ^2H_2O, pD 5.5.

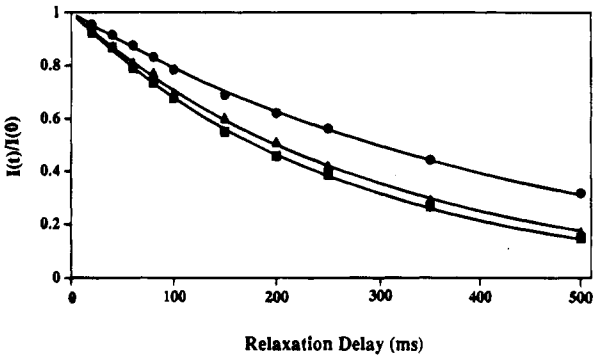

Figure 2. Representative $R_{1zz}(H,C)$ decay curves. Normalized experimental data points for Tyr-1, Asp-5, and Ala-9 are indicated by ▲, ■, and ● symbols, respectively. The solid lines represent best-fits of the experimental data to exponential decays.

Determination of the Model-Free Parameters. Quantitative dynamic information was obtained by fitting the relaxation data to the model-free spectral density functions (eq 7–9). Before

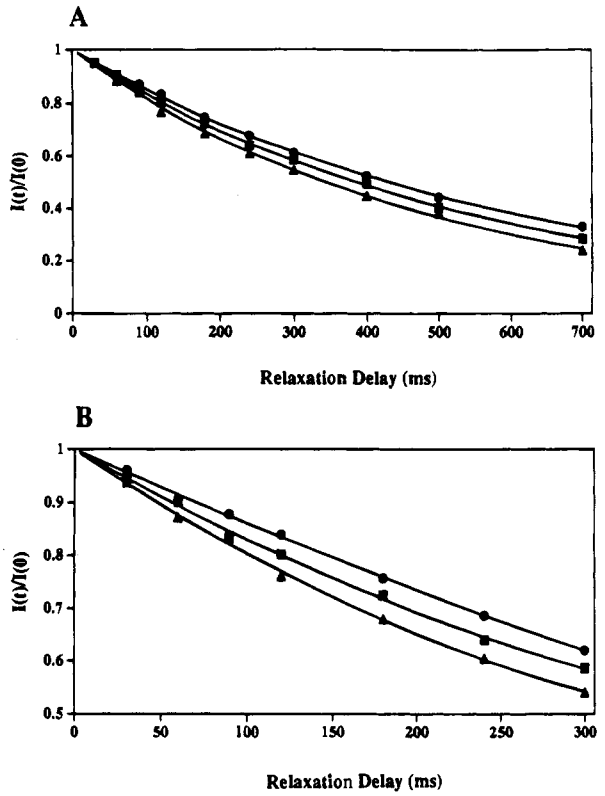

Figure 3. Representative R_1(H) decay curves. Normalized experimental data points for Tyr-1, Pro-4, and Ala-9 are indicated by ▲, ■, and ● symbols, respectively. (A) Fits of all 10 time points to exponential decays. The solid lines represent best-fits to the experimental data. (B) Fits of the first seven time points to second order Taylor series expansions. The solid lines represent best-fits to the experimental data.

describing this analysis, a caveat should be made. To characterize the global motion of the peptide in terms of a single overall correlation time τ_r, the tumbling motion must be reasonably isotropic and independent of internal motions. These conditions are usually well satisfied for globular proteins but become important issues for peptides. The principle moments of the inertial tensor for the 24 X-PLOR generated models (preceding article in this issue) are (1.00):(1.21 ± 0.16):(1.29 ± 0.14), indicating the assumption of isotropic tumbling is valid provided the β-hairpin is the predominant conformation. Indeed, the NOESY data and modeling evidence strongly suggest the full β-hairpin is highly populated (preceding article in this issue). This assertion is further supported by the relatively uniform $\{^1H\}-^{13}C$ NOE values and R_1(C) rates observed for residues 2 thru 8 (Table 1). However, we cannot assume τ_r is independent of internal motions. This issue is critically addressed in the **Discussion** section below. The order parameters and correlation times should still be meaningful reflections of the relative degrees of conformational restriction and motional time scales among the residues. These considerations were further examined by using a second fitting protocol which treats τ_r as a local, rather than a global, parameter.

A preliminary estimate of the global τ_r was obtained from the R_2(C)/R_1(C) ratios of residues 2, 4, 5, 7, and 8, assuming the spectral densities given are by eq 7. Residues 1 and 9 were excluded because their $\{^1H\}-^{13}C$ NOEs and R_1(C) and Δ_z relaxation rates (Table 1) indicate high picosecond−nanosecond time scale mobility. Residue 3 was excluded due to the relatively large errors associated with its relaxation observables. This analysis afforded a preliminary estimate of the global τ_r of 0.87 ± 0.10 ns. This value was used as the initial estimate

Table 2. Relaxation Parameters for the Methine $H^\alpha-C^\alpha$ Groups of Y-Q-N-P-D-G-S-Q-A Obtained from Fitting R_1(C), R_2(C), and the NOE, with τ_r Fixed at 0.93 ns

residue	model[a]	S^2 [b]	τ_i[c] (ps)	R_{2ex} (s^{-1})	χ^2
Tyr-1	2	0.60 ± 0.02	94 ± 12		0.098
Gln-2	1	0.82 ± 0.02			4.910
Asn-3	1	0.91 ± 0.04			1.035
Pro-4	1	0.81 ± 0.01			4.470
Asp-5	1	0.84 ± 0.001			1.855
Ser-7	2	0.73 ± 0.01	45 ± 8		0.097
Gln-8[d]	2	0.67 ± 0.03	63 ± 10		5.940
	3	0.34 ± 0.03	1090 ± 150		0.009
Ala-9	2	0.39 ± 0.02	60 ± 6	2.01 ± 0.16	0.000

[a] Refers to the spectral density function used in the fit. Modes 1, 2, and 3 correspond to eqs 7, 8, and 9, respectively. [b] Refers to $S_f^2S_s^2$ if model 3 was used. [c] Refers to the internal correlation time, i.e., τ_e if model 2 was used, τ_s if model 3 was used. [d] The fitting of Gln-8 proved problematic. Use of model 2 yielded physically reasonable parameters, but the χ^2 value is above the critical value (3.843) for the 95% confidence limit. Model 3 yielded a good fit but produced a physically questionable τ_s. See text for further discussion.

Table 3. Relaxation Parameters for the Methine $H^\alpha-C^\alpha$ Groups of Y-Q-N-P-D-G-S-Q-A Obtained from Fitting R_1(C), R_2(C), Δ_z, and the NOE, with τ_r Fixed at 0.93 ns

residue	model[a]	S^2 [b]	τ_i[c] (ps)	R_{2ex} (s^{-1})	χ^2
Tyr-1	2	0.61 ± 0.02	93 ± 10		0.239
Gln-2	2	0.77 ± 0.02	53 ± 16		2.195
Pro-4	1	0.78 ± 0.02		0.37 ± 0.22	5.084
	2	0.78 ± 0.02	32 ± 16		4.607
Asp-5	1	0.84 ± 0.01			1.941
Ser-7	2	0.73 ± 0.01	46 ± 8		0.187
Gln-8[d]	2	0.68 ± 0.03	60 ± 19		6.258
	3	0.67 ± 0.03	75 ± 22		6.207
Ala-9	2	0.39 ± 0.02	59 ± 5	2.00 ± 0.17	0.651

[a] Refers to the spectral density function used in the fit. Models 1, 2, and 3 correspond to eqs 7, 8, and 9, respectively. [b] Refers to $S_f^2S_s^2$ if model 3 was used. [c] Refers to the internal correlation time, i.e., τ_e if model 2 was used, τ_s if model 3 was used. [d] The fitting of Gln-8 proved problematic. Models 2 and 3 without R_{2ex} included yielded the best fits and physically reasonable parameters, although both had χ^2 above the 95% confidence limit. See text for further discussion.

for a global fitting of τ_r. A more accurate estimate of τ_r was obtained via minimization of eq 12, with the sum extending over the $\{^1H\}-^{13}C$ NOEs and R_1(C) and R_2(C) relaxation rates of residues 2, 4, 5, 7, and 8. The spectral densities were of the form given in eq 8, with independent S^2 and τ_e values used for each residue. The resulting S^2 and τ_e values indicate increasing mobility as residues near the termini are approached from the peptide's center. These S^2 and τ_e values will not be discussed further, since the global fitting is primarily intended to optimize the global τ_r. The global τ_r value obtained with this approach is 0.93 ± 0.03 ns, with the error bounds determined by Monte Carlo analysis. The χ^2 for the fit is 9.51, which is near the 95% confidence level for a fit with 4 degrees of freedom (9.49).

Fixing τ_r at 0.93 ns, the model-free parameters were fit to the relaxation observables for each residue independently, as described in the **Materials and Methods** section. The results of this analysis are given in Tables 2 and 3, which present parameters obtained without and with Δ_z included in the fits, respectively. In Table 2, the S^2 values range from 0.39 (Ala-9) to 0.91 (Asn-3), excluding the physically unrealistic result obtained for Gln-8 (see **Discussion**). The same fits were also performed with τ_r treated as a variable, residue-specific (local) parameter. These results are presented in Tables 4 and 5. Table 4 gives the parameters obtained without Δ_z included in the fits, and Table 5 gives the parameters obtained with Δ_z included.

Table 4. Relaxation Parameters for the Methine $H^{\alpha}-C^{\alpha}$ Groups of Y-Q-N-P-D-G-S-Q-A Obtained from Fitting $R_1(C)$, $R_2(C)$, and the NOE, with τ_r Treated as an Adjustable Parameter

residue	model[a]	S^2 [b]	τ_e (ps)	R_{2ex} (s^{-1})	τ_r (ns)	χ^2
Tyr-1	1	0.81 ± 0.02		0.82 ± 0.16	0.49 ± 0.08	0.012
	2	0.60 ± 0.03	92 ± 11		0.95 ± 0.08	0.059
Gln-2	1	0.84 ± 0.02			0.84 ± 0.05	1.886
Asn-3	1	0.91 ± 0.05			0.98 ± 0.14	0.971
Pro-4	1	0.81 ± 0.02			0.97 ± 0.05	3.841
Asp-5	1	0.85 ± 0.02			0.91 ± 0.05	1.585
Ser-1	1	0.79 ± 0.02		0.65 ± 0.15	0.68 ± 0.03	0.009
	2	0.73 ± 0.02	45 ± 8		0.94 ± 0.05	0.057
Gln-8	1	0.82 ± 0.03			0.65 ± 0.05	1.338
Ala-9[c]	1	0.63 ± 0.02		2.57 ± 0.16	0.39 ± 0.02	0.004
	2	0.44 ± 0.02	81 ± 7		1.84 ± 0.09	0.051

[a] Refers to the spectral density function used in the fit. Models 1 and 2 correspond to eqs 7 and 8, respectively. [b] Refers to $S_f^2S_s^2$ if model 3 was used. [c] Although the fit for Ala-9 using model 2 without R_{2ex} yields a good fit, a physically unreasonable τ_r is produced. See text for further discussion.

Table 5. Relaxation Parameters for the Methine $H^{\alpha}-C^{\alpha}$ Groups of Y-Q-N-P-D-G-S-Q-A Obtained from Fitting $R_1(C)$, $R_2(C)$, Δ_z, and the NOE, with τ_r Treated as an Adjustable Parameter

residue	model[a]	S^2 [b]	τ_e (ps)	R_{2ex} (s^{-1})	τ_r (ns)	χ^2
Tyr-1	2	0.60 ± 0.02	93 ± 9		0.95 ± 0.07	0.164
Gln-2	1	0.83 ± 0.02		0.54 ± 0.21	0.71 ± 0.04	0.492
	2	0.77 ± 0.03	51 ± 23		0.92 ± 0.07	2.150
Pro-4	1	0.79 ± 0.02		0.77 ± 0.25	0.78 ± 0.07	0.005
	2	0.75 ± 0.02	46 ± 17		1.06 ± 0.06	0.758
Asp-5	1	0.85 ± 0.02			0.91 ± 0.05	1.742
Ser-7	1	0.80 ± 0.02		0.54 ± 0.17	0.70 ± 0.03	2.463
	2	0.73 ± 0.02	46 ± 9		0.94 ± 0.06	0.171
Gln-8	1	0.82 ± 0.03			0.66 ± 0.04	1.443
Ala-9[c]	2	0.44 ± 0.02	80 ± 7		1.85 ± 0.08	0.006

[a] Refers to the spectral density function used in the fit. Models 1 and 2 correspond to eqs 7 and 8, respectively. [b] Refers to $S_f^2S_s^2$ if model 3 was used. [c] Although the fit for Ala-9 using model 2 without R_{2ex} yields a good fit, a physically unreasonable τ_r is produced. All other fits yield high χ^2 or physically unreasonable τ_r values. See text for further discussion.

Figure 4. Stereoview of 100 superimposed structures taken from the unrestrained MD run, showing the backbone N, C, and C^{α} atoms. These structures were taken at evenly spaced intervals during the 1.40 ns production run. The N-terminus is located at the lower left region of the figure.

Conformers Produced by the Molecular Dynamics Simulation. The MD run was performed at 278 K, which corresponds to the experimental temperature at which the solution conformation (preceding article in this issue) and backbone dynamics were characterized. The backbone-atom RMSD to the starting conformation fluctuates between about 1.0 and 2.0 Å during the 1.40 ns production run (data not shown).

In Figure 4, 100 structures saved at equally spaced intervals during the 1.40 ns production run are shown. While significant local conformational variability is observed (especially for residues Tyr-1, Gly-6, Ser-7, Gln-8, and Ala-9), it is clear that the overall β-hairpin fold is maintained. The average backbone atom and all heavy atom RMSDs of the Figure 4 structures to the mean coordinates over this part of the trajectory are 0.78 and 1.29 Å, respectively. These structures are quite similar to a set of structures produced previously by ensemble-averaged molecular modeling (preceding article in this issue), both in terms of average conformation and conformational disorder. This latter set was produced with a "mixed" set of distance restraints, with some treated in the ensemble-averaged fashion and some treated in the standard "static" manner. If the mean coordinates of the set of structures produced with the mixed constraints (preceding article in this issue) are compared to the mean coordinates of the MD snapshots (Figure 4), the backbone atom and all heavy atom RMSDs are 0.77 and 1.25 Å, respectively. Important interactions observed during the MD run include backbone−backbone H-bonds between Tyr-1 O and Ala-9 H^N (51% populated) and between Asn-3 H^N and Ser-7 O (75% populated). The side chain of Asn-3 is involved in H-bonding interactions with Asp-5, Gly-6, and Ser-7. For the most part, these results are consistent with H-bonding interactions revealed by ensemble-averaged molecular modeling (preceding article in this issue). The H-bond between Asn-3 O and Gly-6 H^N is a notable exception, since it is only 17% populated in the MD simulation, whereas the ensemble-averaged modeling consistently indicated a population of more than 50% for this H-bond.

Order Parameters from the Molecular Dynamics and NMR-Based Modeling Data. Table 6 lists consensus values for the experimental $H^{\alpha}-C^{\alpha}$ S^2 values derived from Tables 2 and 3, S^2 values derived from the MD simulation, and S^2 values derived from three sets of structures computed with CONGEN[19] (preceding article in this issue).

With the exception of Ser-7, the agreements between the experimental and MD-derived S^2 values are quite good.

(19) (a) Bruccoleri, R. E.; Karplus, M. *Biopolymers* **1987**, *26*, 137−168. (b) Bruccoleri, R. E.; Haber, E.; Novotny, J. *Nature* **1988**, *335*, 564−568. (c) Bruccoleri, R. E. *CONGEN (Version 2.0) Manual*; Bristol-Myers Squibb Pharmaceutical Research Institute, Princeton, NJ, 1992. (d) Bruccoleri, R. E. *Molecular Simulation* **1993**, *10*, 151−174.

Excluding Ser-7, the magnitude of the average S^2 difference is 0.04 ± 0.04. The MD-derived S^2 value of Ser-7 (0.32) is much lower than the experimental value (0.73). This reflects the behavior of the ψ angles of Gly-6 and Ser-7. The Gly-6 ψ angle fluctuates rapidly between $\sim +80°$ and $\sim -90°$ for about the first 1.0 ns of the production run. At this point, a conformational transition occurs, with the Gly-6 ψ angle fluctuating near $\sim -105°$ for the remainder of the simulation. The Ser-7 ψ angle also undergoes large-scale transitions at ~1.0 ns into the production run, fluctuating near 140° prior to the transition, and fluctuating near $\sim -60°$ after the transition. Such a situation can result in anomalously low MD-derived S^2 values, especially if the conformational transitions occur more frequently in the MD simulation than they do in the real experimental system.[20] When a 0.28 ns sliding window is applied in the calculation, the Ser-7 S^2 value becomes 0.68, in reasonable accord with the experimental value.

Regarding the CONGEN structures (preceding article in this issue), set 1 was computed using standard constraints, set 2 was computed using all ensemble-averaged constraints, and set 3 was computed with a mixture of standard and ensemble-averaged constraints. The 60 structures from the 30 lowest energy 2-member ensembles were retained in the final set for sets 2 and 3; for set 1, the 60 lowest-energy structures out of 120 total structures were retained.

For set 1, all of the structure-derived order parameters are higher than the experimental values, with the largest deviations occurring for Tyr-1, Gln-8, and (especially) Ala-9. The average S^2 difference (experimental *minus* structure-derived) is -0.24 ± 0.16. All characterized residues, except Ser-7, have S^2 values > 0.95. The only experimentally characterized $H^\alpha-C^\alpha$ vector for which the set 1 structures show a moderately reduced S^2 is Ser-7, for which the structure-derived S^2 value still exceeds the experimental value by ~0.1. The set 2 structures show the opposite trend: the order parameters derived from the structures are all much lower than the experimental values. The average difference between the experimental and structure-derived S^2 values is 0.39 ± 0.11. For the set 3 structures, relatively good agreement with the experimental results is obtained: the average S^2 difference is 0.08 ± 0.09. If the residues are divided into three classes based on the S^2 values—relatively rigid ($0.80 < S^2 < 1.00$), intermediate flexibility ($0.50 < S^2 < 0.80$), and highly mobile ($S^2 < 0.50$)—complete agreement is obtained. The largest discrepancy between the experimental and set 3 structure-derived S^2 values is observed for Ala-9, which has an extremely low structure-derived S^2 value of 0.09. This is discussed further below.

Discussion

Motional Properties Based on the ^{13}C Relaxation Analysis. Four different protocols were used to fit the relaxation data—the data were fit with and without Δ_z and with τ_r fixed at 0.93 ns or with τ_r treated as a local, adjustable parameter. This rather extensive treatment was needed in order to judge the suitability of the model-free approach and to ascertain the reliability of the Δ_z observable, which may contain systematic errors due to nonexponential decays and dipolar/CSA cross-correlation effects. In this way, general features of the residue-specific motional properties are revealed. In what follows, the results for each characterized residue are discussed.

Using three observables and with τ_r fixed (Table 2), Tyr-1 was adequately fit by one two-parameter model (eq 8). This analysis yielded S^2 and τ_e values of 0.60 and 94 ps, respectively. Nearly identical values were obtained using four observables and with τ_r fixed (Table 3), demonstrating that Δ_z is consistent with the remaining observables. With three observables and allowing τ_r to vary (Table 4), two three-parameter models adequately fit the data: eq 7 with R_{2ex} and eq 8. In the former case, a "compensation effect" is observed wherein S^2 increases and τ_r decreases to well below the derived global value. The decrease in τ_r is consistent with enhanced flexibility on a picosecond–nanosecond time scale; e.g., it is analogous to the decrease in local correlation times observed (using the single local correlation time approximation[4b]) in organic polymers as one moves away from branch points. Equation 7 requires a moderate R_{2ex} contribution to fit the data. The second model (eq 8) yields S^2 and τ_e values very similar to those obtained with τ_r fixed, and the local τ_r (0.95 ns) is very close to the global value, suggesting that this model provides a more realistic description of the motion. This contention is further supported by the data reported in Table 5, since the only three-parameter model that adequately fits the data is eq 8. Thus, the R_{2ex} reported in Table 4 for Tyr-1 is probably an artifact of an inappropriate model. It is clear that the Tyr-1 backbone displays substantial internal motion on the picosecond time scale, as demonstrated by $S^2 = 0.60-0.61$ for most models.

Gln-2 was adequately fit by the one-parameter model (eq 7) using three observables and with τ_r fixed (Table 2), with an S^2 value of 0.82. In all cases, for all models that yielded an adequate fit, the S^2 value was found to lie between 0.77 and 0.84. A small R_{2ex} contribution was found in one case (Table 5); however, as with Tyr-1, this R_{2ex} contribution is probably spurious. Overall, the data indicate that the Gln-2 backbone is moderately well ordered on the picosecond time scale. In the case of Asn-3, Δ_z was not measurable. With τ_r fixed (Table 2), a one-parameter model (eq 7) yields an adequate fit, with $S^2 = 0.91$. With τ_r adjustable (Table 4), S^2 was 0.91, and the local τ_r was 0.98 ns, which is close to the global value. These data indicate that the Asn-3 backbone is highly ordered.

The S^2 value of Pro-4 was found to lie between 0.75 and 0.81 for all cases that yielded an adequate fit. Fits based on eq 7 gave small-to-moderate exchange contributions when Δ_z was included (Tables 3 and 5), but the use of eq 8 without R_{2ex} also adequately fit the data. While slower motions cannot be absolutely ruled out, they are unlikely. The Pro-4 backbone appears to be relatively well ordered on the picosecond–nanosecond time scale. The next residue, Asp-5, displays the most consistent fitting results of any residue. In all cases, eq 7 was found to yield adequate fits, with S^2 values between 0.84 and 0.85. In both cases where τ_r was adjustable (Tables 4 and 5), the local τ_r was found to be 0.91 ns, which is very close to the global value. Thus, Asp-5 appears to be well ordered. This result is consistent with a stable turn spanning residues 3–6.

The data for Ser-7 yielded S^2 values of 0.73 for all cases in which eq 8 was found to produce an adequate fit (Tables 2–5). Also, a τ_e of 45–46 ps was consistently obtained in these cases. When τ_r was allowed to float (Tables 4 and 5), eq 7 with R_{2ex} was also found to fit the data. These fits exhibited the above-mentioned "compensation effect" between S^2 and τ_r, with S^2 increasing to ~0.80 and τ_r decreasing to ~0.69 ns. Again, these latter results may reflect an inappropriate model, and the R_{2ex} contributions may be artifactual. Overall, the data indicate that Ser-7 is a borderline case, showing an intermediate degree of disorder on the picosecond–nanosecond time scale.

Gln-8 proved to be an interesting case. Using three observables and with τ_r fixed, both two-parameter models failed to give an adequate fit. In Table 2, we report the results obtained using eq 8, which gave the best, albeit inadequate two-parameter

(20) Fushman, D.; Ohlenschlager, O.; Ruterjans, H. *J. Biomolec. Struct. Dynamics* **1994**, *11*, 1377–1402.

fit. This analysis yielded a S^2 value of 0.67 and a τ_e of 63 ps. The only model that yielded an good fit was eq 9, a three-parameter model. This analysis yielded a S^2 value of 0.34 and a τ_s of 1090 ps. This is a physically questionable result, since τ_s is greater than τ_r. With τ_r fixed and all four observables included, no models could produce an adequate fit. Table 3 reports results obtained with eqs 8 and 9, which produced the lowest (but still less than adequate) χ^2 values with τ_r fixed. Both models gave S^2 values of ~0.67 and internal correlation times of 60−75 ps. Acceptable fits were readily produced when τ_r was treated as an adjustable parameter (Tables 4 and 5). Using eq 7, this analysis yielded a S^2 value of 0.82 and a local τ_r of 0.65−0.66 ns. This is another example of the S^2/τ_r compensation effect noted above. The reduced τ_r (relative to the global value) indicates enhanced picosecond−nanosecond timescale motions. Taken together, these results suggest that Gln-8 may experience time scale-separated internal motions, with the slower motions occurring on a time scale comparable to τ_r. In any case, Gln-8 displays complex relaxation behavior that is inconsistent with highly restricted internal motion on the picosecond−nanosecond time scale.

Ala-9 appears to be the most mobile residue in the peptide. With τ_r fixed, the only model that resulted in an adequate fit was a three-parameter model, eq 8 with a R_{2ex} contribution (Tables 2 and 3). This analysis yielded a S^2 value of 0.39, a τ_e of 59−60 ps and a R_{2ex} of ~2.0 Hz. The fitting of the Ala-9 data was more problematic when τ_r was allowed to vary. With Δ_z excluded (Table 4), two three-parameter models adequately fit the data. Using eq 7 with R_{2ex}, a S^2 value of 0.63, a τ_r of 0.39 ns, and a R_{2ex} of 2.57 Hz were obtained. A large S^2/τ_r compensation effect occurs, consistent with large amplitude nanosecond-picosecond time scale motions. The second model that fit the data was eq 8 without R_{2ex} (Tables 4 and 5). This fitting produced a physically unreasonable τ_r of 1.84−1.85 ns. This is approximately twice the derived global τ_r value (0.93 ns). Since R_2(C) is within the range observed for the other residues, global anisotropic motion cannot account for this result. The large τ_r is needed to reproduce the observed R_2(C) value (Table 1) without including R_{2ex} in the fitting. Clearly, this is an inappropriate model. Overall, the data indicate that Ala-9 is highly mobile on the picosecond−nanosecond time scale. Furthermore, all models that produce both adequate fits and physically reasonable parameters include a large (2.0−2.6 Hz) R_{2ex} contribution, suggestive of substantial motions on the microsecond−millisecond time scale. Alternatively, it may be that all of the model-free functional forms used do not appropriately describe the $J(0)$ spectral density function of Ala-9, which dominates the R_2 relaxation behavior (eq 2). Given its mobility and location within the peptide, alternate orientations of Ala-9 (e.g., see Figure 8 of the preceding article in this issue) may, depending on their interconversion time scale, couple to the global τ_r value, rendering any description based on separable internal and global motions inadequate for this residue.

In summary, the results of this analysis indicate that motions on the picosecond−nanosecond time scale are relatively restricted for residues 2, 3, 4, and 5, and that residues 1, 7, 8, and 9 have higher flexibility on this time scale. Slower nanosecond−millisecond time scale motions may also influence the relaxation behavior of residue 9. When τ_r is held fixed, there is a general tendency for the amplitudes of the local motions to increase as one moves out from the center of the peptide toward the C-terminus. Excluding Tyr-1, the N-terminal half of the peptide is well ordered. When τ_r is allowed to vary, the "local correlation times" tend to decrease toward the ends of the peptide, indicating enhanced mobility on the nanosecond−picosecond time scale for the termini. Such results are expected on theoretical grounds even for relatively rigid peptides.[21]

Comparison of Relaxation, Molecular Dynamics, and NMR-Based Modeling Data. The values of S^2 reflect the distribution of conformational states that interconvert over time scales on the order of τ_r or faster. Ideally, the distribution of conformations obtained from a MD simulation, or from an NMR structure determination, should reflect the actual distribution of conformational states sampled by the system. A comparison of experimental S^2 values with S^2 values derived from a set of structure provides a measure for the adequacy of the conformational sampling; i.e., one can determine if a set of structures are at the appropriate level of precision. Alternatively, a set of structures that reproduces the experimental S^2 values affords a clear visualization of the accessible conformations without resorting to specific motional models in the interpretation of S^2. For example, this approach has recently been used to compare active site loop conformations observed in an ensemble of NMR structures of the protein echistatin to experimentally derived order parameters.[22] The comparison of experimental and structure derived S^2 values provides a link between the modeling and relaxation data. As discussed in detail below and in ref 22, such a comparison is rigorous if motions slow with respect to τ_r do not contribute extensively to the conformational sampling. If a set of structures accurately reflects both rapidly and slowly interconverting conformers, the structure-derived S^2 values will be lower than the experimental values. Since this issue is of central importance to the characterization of the β-hairpin peptide and to the characterization of structural ensembles in general, further analysis is warranted.

To begin with, all of the experimental data−the $^1H-^1H$ NOEs, ^3J coupling constants, and ^{13}C relaxation data−were acquired on a system under conditions of *dynamic equilibrium*. The various NMR-based modeling protocols used (preceding article in this issue) were designed to produce distributions of conformers that implicitly reflect the motional averaging that takes place in solution. The generalized order parameter S^2 is, by definition, an *equilibrium* property; it is given by the limiting (plateau) value of the autocorrelation function $G(t)_{int}$ reflecting reorientations of the internuclear vector in the molecular frame

$$S^2 = \lim_{t\to\infty} G(t)_{int} = (4\pi/5) \sum_{m=-2}^{m=2} |\langle Y_{2,m}(\theta,\phi)\rangle|^2 \quad (14)$$

where $Y_{2,m}$ are second-order spherical harmonics, and θ and ϕ describe the orientation of the internuclear vector in the internal (molecular) frame. The right-hand side of eq 14 is equivalent to eq 13. Thus, as defined, S^2 reflects the *equilibrium distribution* of conformational states. As stated by Lipari and Szabo,[8a] "the generalized order parameter can be expressed as an equilibrium average and contains no information about the time scale of the dynamics; it is solely a measure of the spatial restriction of the motion". Since we are dealing with a system at equilibrium, it is expected to obey the ergodic hypothesis.[23] Thus, computing S^2 according to the definition (eqs 13 and 14) from an ensemble of independently produced conformers is as valid as computing S^2 from a series of snapshots recording during a long MD simulation of a single system. The long MD simulation has the advantage that the conformational behavior

(21) Perico, A.; Guenza, M.; Mormino, M.; Floravanti, R. *Biopolymers* **1995**, *35*, 47−54.

(22) Chen, Y.; Suri, A. K.; Kominos, D.; Sanyal, G.; Naylor, A. M.; Pitzenberger, S. M.; Garsky, V. M.; Levy, R. M.; Baum, J. *J. Biomolec. NMR*, **1994**, *4*, 307−324.

(23) McQuarrie, D. A. *Statistical Mechanics*; Harper and Row: New York, 1976, pp 554.

can be monitored through time as well as space. This may become important when comparing to experimental relaxation data (see below).

One of the main challenges addressed here and in the preceding article in this issue involves identifying which of the conformational distributions obtained by modeling most closely resembles the real conformational distribution in solution. The problem with comparing results from modeling (either from an NMR-based ensemble or snapshots saved from an MD simulation) with experimental relaxation data is that S^2, as defined above, is only experimentally measurable under certain conditions. The experimentally determined S^2 value is directly comparable to the limiting value of $G(t)_{int}$ if $G(t)_{int}$ decays at a rate faster than the overall tumbling rate of the molecule. The reason for this is due to the fact that the measured relaxation rates are linear combinations of the spectral densities, which in turn are Fourier transforms involving the total (laboratory frame) autocorrelation functions $G(t)_{tot}$. In its simplest model-free form, $G(t)_{tot}$ is given by[8a]

$$G(t)_{tot} = \exp(-t/\tau_r)G(t)_{int} = \exp(-t/\tau_r)\,[S^2 + (1 - S^2)\exp(-t/\tau_e)] \quad (15)$$

Although this is an idealized representation, it captures the essential physics of the situation. As t approaches infinity, $G(t)_{int}$ approaches S^2, as required. However, the decay of $G(t)_{tot}$ becomes progressively less sensitive to $G(t)_{int}$, and thus less sensitive to S^2, as the time scale of the internal motion increases. In practice, this means that the experimentally derived S^2 parameters reflect only rapid motions and *therefore represent a lower limit on the actual degree of disorder present.* It follows that any ensemble of conformational models that accurately represents the actual conformational distribution sampled by the real system should yield S^2 values that are similar to, or lower than, the experimental values. If slow motions with significant amplitudes occur, a realistic ensemble will produce lower S^2 values than experiment; if all significant motions occur on fast time scales, a realistic ensemble will produce S^2 values similar to those determined by experiment. It is in this context that a single long MD simulation has an advantage over independently produced structures, since sliding time windows can be applied to the calculation of order parameters in the former case.

For the β-hairpin peptide, the fits of the ^{13}C relaxation data for most residues yielded internal correlation times of less than 100 ps (see Tables 2–5), indicating that fast internal motions predominate the relaxation-active dynamics for most residues. Gln-8 and Ala-9 may experience slower motions, so comparing experimental and model-based parameters for these residues must be done with caution.

Order parameters derived from the MD snapshots and the set 3 CONGEN structures (preceding article in this issue) agree rather well overall with the experimental data (Table 6). For the set 1 CONGEN structures, the comparison clearly shows that this set of structures computed with standard (nonensemble-averaged) constraints is overly precise. This demonstrates the danger of interpreting cross-relaxation rates and ^3J values as static constraints (i.e., as constraints that must be satisfied by a single conformation) when modeling relatively flexible systems. On the other hand, the set 2 CONGEN structures appear to be overly imprecise. In order to reconcile the discrepancy between the experimental and set 2 S^2 values, one must postulate that large amplitude, slow (~ns to ms timescale) interconversions among well populated conformers occur for the entire peptide backbone. This is inconsistent with the relaxation data, since the only residues showing significant evidence of slow motions are Gln-8 and Ala-9. These results confirm that ensemble-averaging all constraints can lead to an unrealistically wide sampling of the conformational space.

Table 6. Comparison of Experimental and Structure-Derived Generalized Order Parameters for the $H^\alpha-C^\alpha$ Vectors

residue	S^2 exp[a]	S^2 MD[b]	S^2 set 1[c]	S^2 set 2[d]	S^2 set 3[e]
Tyr-1	0.61	0.55	0.97	0.16	0.61
Gln-2	0.81	0.84	0.98	0.53	0.85
Asn-3	0.91	0.93	0.98	0.33	0.86
Pro-4	0.79	0.81	0.97	0.27	0.67
Asp-5	0.84	0.85	0.96	0.54	0.86
Ser-7	0.73	0.32	0.84	0.36	0.64
Gln-8	0.67	0.66	0.96	0.38	0.60
Ala-9	0.39	0.27	0.98	0.08	0.09

[a] "Consensus value"—average of all realistic experimental values from Tables 2 and 3. [b] Derived from MD simulation. The order parameters reported were computed using a window size equal to the trajectory length (1.40 ns). [c] Set of 60 CONGEN structures produced with standard constraints (see accompanying article). [d] Set of 60 CONGEN structures from 30 two-member ensembles produced with all ensemble-averaged constraints (see accompanying article). [e] Set of 60 CONGEN structures from 30 two-member ensembles produced with the mixed set of standard and ensemble-averaged constraints (see accompanying article).

Gln-2 through Asp-5 comprise the most rigid region of the peptide, as indicated by the S^2 values derived from the experimental relaxation data, the MD simulation, and the set 3 CONGEN structures. As mentioned above, Ala-9 shows evidence of significant mobility on the nanosecond–millisecond time scale, in addition to large amplitude motions on the ~50–100 picosecond time scale. Therefore, the low structure-derived S^2 values for this residue (Table 6) are not inconsistent with the experimental results. Overall, the set 3 CONGEN structures and the MD snapshots appear to display the correct level of precision. Given the additional consistency obtained with respect to the experimental $^1H-^1H$ NOE and ^3J-coupling data (see preceding article in this issue), it is likely that the set 3 CONGEN structures are a reasonably accurate representation of the conformational space spanned by the peptide in solution. This set has well populated backbone–backbone hydrogen bonds involving Asn-3, Gly-6, and Ser-7, less populated hydrogen bonding interactions involving the Asn-3 side chain, and highly variable interactions between the N- and C-terminal residues.

Applicability of the Model-Free Formalism. The model-free approach yielded reasonably good fits to the relaxation data. However, a number of questions remain regarding the validity of this approach when applied to peptides, particularly the issue of the separability of global and internal motions.[24] The fundamental question is whether or not the total correlation function can be approximated as a product of a correlation function for overall rotation and an internal correlation function, as in eq 15 above. The issue becomes less important with increasing molecular size, as local conformational changes have a negligible effect on the overall hydrodynamic behavior of the system. The issue also becomes less important for motions occurring much faster than the overall tumbling time, since all of the molecules will display the same average hydrodynamic surface during a rotational period. Motions that occur on time scales comparable to the overall tumbling rate can potentially couple to the overall motion. In such cases, the product approximation breaks down. The following considerations indicate that, at least as far as order parameters are concerned, the application of model-free formalisms to this system is

(24) Abseher, R.; Ludemann, S.; Schreiber, H.; Steinhauser, O. *J. Am. Chem. Soc.* **1994**, *116*, 4006–4018.

justified, particularly for residues 1−7. First, the structural modeling (preceding article in this issue) and relaxation results indicate that the population of unfolded conformers is low and that all of the folded conformers fall within a manifold of β-hairpin structures. These should all have similar hydrodynamic volumes, and they should behave in a reasonably isotropic manner. This contention is supported by the fact that when τ_r is treated as a local parameter rather than a global parameter, all residues except Gln-8 and Ala-9 yield values that are close to the global value of 0.93 ns (Tables 4 and 5). Second, as discussed above, the significant internal motions of most residues occur on time scales < 100 ps, which is an order of magnitude faster than the overall tumbling time. Finally, a recent publication[25] presented a detailed ^{13}C relaxation study of a single $C^{\alpha}-H^{\alpha}$ vector in the peptide motilin under a variety of conditions. Even under conditions where the overall model-free approach failed, it still gave meaningful order parameters. The result that most of the experimental order parameters for the β-hairpin peptide are reproduced rather well by the MD simulation (Table 6) also supports the validity of the model-free approach.

While these considerations *indicate* that the model-free approach should be valid for most residues, they do not *prove* it. To further address these issues, we are attempting to extend the solvated MD simulation to 10−20 ns. This will allow a direct simulation of the total autocorrelation functions, spectral densities and relaxation rates, without the necessity of assuming any particular motional model. Thus, a comparison of order parameters derived directly from the simulation (via eqs 13 and 14) with order parameters produced by fitting simulated relaxation rates to model-free spectral densities will be possible. The results of this work will be presented in a future report.

(25) Allard, P.; Jarvet, J.; Ehrenberg, A.; Graslund, A. *J. Biomolec. NMR* **1995**, *5*, 133−146.

Concluding Remarks

^{13}C relaxation measurements, in conjunction with a "model-free" analysis of the primary relaxation data, have demonstrated relatively high rigidity for residues Gln-2 through Asp-5 of the β-hairpin forming linear peptide Y-Q-N-P-D-G-S-Q-A. More pronounced dynamic behavior has been demonstrated for Tyr-1, Ser-7, Gln-8, and, in particular, Ala-9. The data are consistent with a predominance of β-hairpin-like conformations under the experimental conditions employed. The experimentally derived order parameters were found to be reasonably consistent with a set of structures derived from ensemble-averaged modeling (preceding article in this issue), and with the results of an unrestrained, water-solvated molecular dynamics simulation. The combined results indicate that many of the interactions that stabilize the hairpin are transient or occur in related, but distinct, conformations. This is particularly true for the hydrophobic, hydrogen-bonding and electrostatic interactions between Tyr-1 and Ala-9. Thus, β-hairpin stabilizing interactions occur over a manifold of conformations, allowing for significant residual flexibility and conformational entropy, as indicated by the S^2 values of residues 1, 7, 8, and 9.[26] This description is reminiscent of those given for protein folding intermediates.[2]

Supporting Information Available: The pulse sequences used for measuring T_{1zz}(H,C) and T_1(H) (2 pages). This material is contained in many libraries on microfiche, immediately follows this article in the microfilm version of the journal, can be ordered from the ACS, and can be downloaded from the Internet; see any current masthead page for ordering information and Internet access instructions.

JA952038V

(26) Akke, M.; Brüschweiler, R.; Palmer, A. G. III *J. Am. Chem. Soc.* **1993**, *115*, 9832−9833.